Exploring Heat Sources Using Gravimetric Data: A Case Study of Magadi Geothermal Prospect, Kenya

Evance Odero*, John Githiri, Maurice K'Orowe

Department of Physics, Jomo Kenyatta University of Agriculture and Technology, Nairobi, Kenya
Email: *evance.obonyo@students.jkuat.ac.ke

Abstract

Understanding the location of the subsurface heat sources is crucial for efficient geothermal resource exploration and exploitation. This study aimed to investigate the faults and the depth to heat sources for a geothermal system in Magadi, southern Rift Valley, through the integration of gravity mapping, 3D Euler deconvolution, and spectral analysis. Gravity mapping is a powerful geophysical method widely used to infer subsurface density variations, which are indicative of geological structures and volcanic intrusions that can be potential heat sources. The Volcano-Tectonic and Fluvial-Deltaic Sedimentation process of the Kenyan rift which encompasses the Magadi basin are responsible for geomorphic and geologic processes in the area. Alkali lava sheets of Magadi plateau trachytes covered with lacustrine sediments characterize 80% of the area. Deeper is the Tanzanian craton basement, overlain by Pliocene to Miocene volcanic and sedimentary rocks. A gravity survey with a data density of 2.375 stations/km^2 produced high-resolution anomaly and total horizontal derivative maps showing gravity highs between −180 mGals to −174 mGals along the eastern zone of the study area. A buried major fault trending N-S was delineated in the mid-upper region of the area by Euler solutions at an average depth of 350 meters. Deeper features associated with possible volcanic dykes and sills gave Euler depth ranges of 0.7 km to 2.2 km. Radial average spectral analysis showed depth to the top of shallow and deep features at 2.4694 km and 5.827 km respectively. The correlation between gravity anomalies, geological structures, and present hot springs supports the hypothesis that volcanic processes have played a significant role in the development of the geothermal system in the study area.

1. Introduction

Nguruman-Magadi area in the west of Lake Magadi falls within the Kenyan Rift System to the south. The 80 km² study area as in **Figure 1** is within a region classified as the unexploited geothermal zone in Kenya (Omenda, 2014). The presence of geothermal surface manifestations such as hot springs in the study area piqued the interest of the study. The subsurface volcanic dense bodies within the Rift System, which are partly associated with geothermal heat sources, can be located by the Gravity geophysical method. The principle of gravity surveying is based on the density contrast of geological formations that cause anomalies in the Earth's gravitational field (Nyakundi, Githiri, & Ambusso, 2017). For geothermal exploration, volcanic centers linked to cooling volcanic intrusion within the subsurface, and evidenced by surface manifestations such as hot springs are of great interest (Mariita & Keller, 2007). Such intrusions have characteristic high densities making them detectable to gravity measurement. Gravity mapping is therefore expected to record relatively high values over the high-density subsurface bodies (Atef, El-Gawad, Zaher, & Farag, 2016). To determine the proper location and extent of anomaly sources, three analytic methods have been incorporated into this study. First, 3-dimensional Euler deconvolution that calculates solutions to the depth of causative bodies has been determined. Second, the
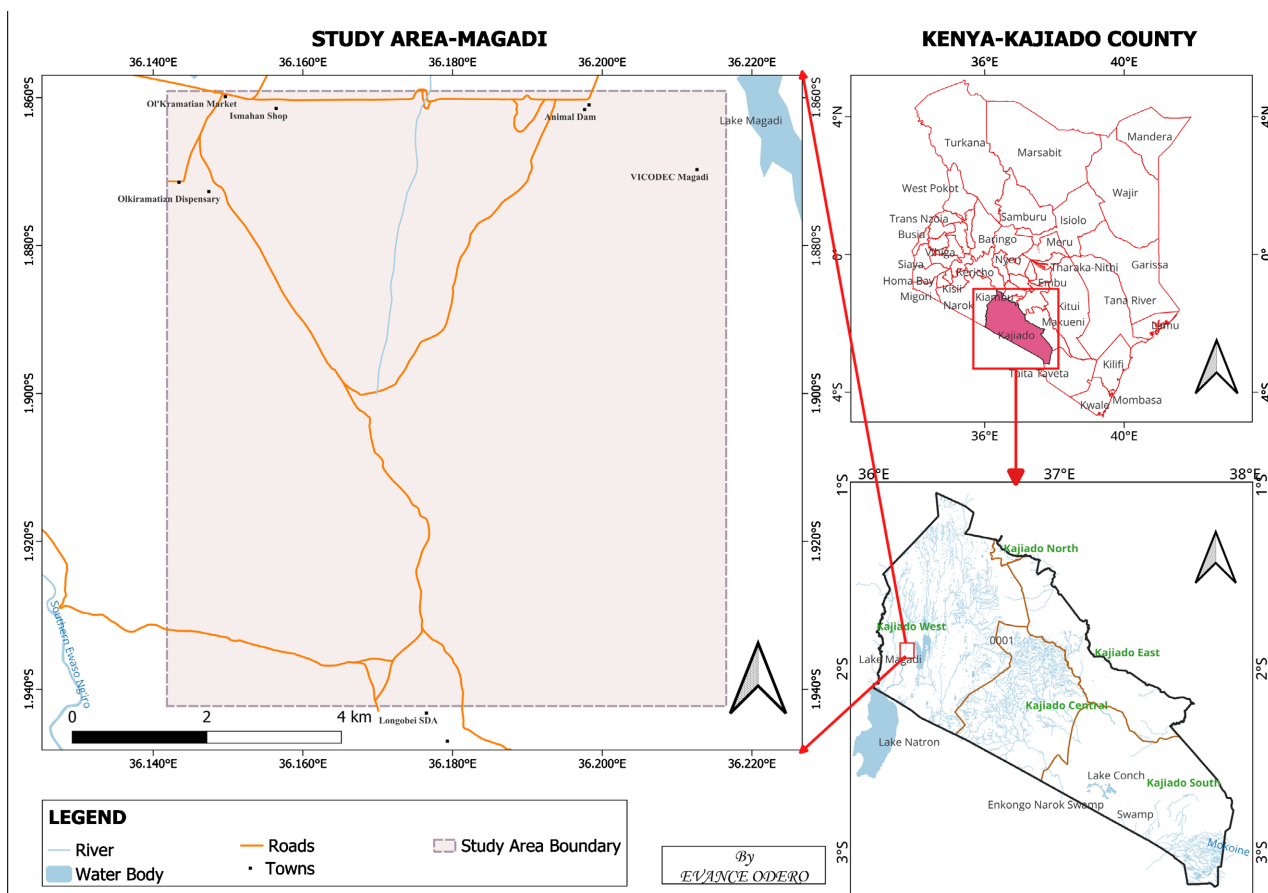

Figure 1. Topographical map of Magadi-Nguruman Study Area, Kajiado county, Kenya.

radial average power spectrum analysis for source body depth discrimination was carried out. Third, the horizontal derivative plot was drawn for extent determination. The three approaches integrate to delineate possible heat sources whose locations could contribute to the determination of the geothermal potential of Magadi. The manner of integration of the analytic methods provides an alternative protocol for processing gravity data for geothermal exploration of unexploited areas such as Magadi.

2. Geology

Kenya Rift System is part of the East Africa Rift System (EARS) which can be traced to worldwide mid-oceanic rift systems. It belongs to the eastern branch of EARS together with Afar, Ethiopia, and Turkana (Omenda, 2007). Stages of Kenyan rift formation began with updoming and volcanism on uplift crests; followed by half-graben faulting to full graben in the early Pleistocene. Basaltic and trachytic lava erupted and flowed over the floor and flanks as observed in places such as Mt. Longonot. These recent eruptions are inferred to have occurred about 140 years ago (Alexander, Ussher, & Merz, 2011). Nguruman-Magadi area in Kajiado County falls within the Kenyan Rift to the south. It shares the general geological setting of the Magadi zone. A model was developed (Muirhead et al., 2016; Simiyu & Keller, 1998) suggesting an existing basement at the bottom of Lake Magadi, which is exposed at the western and eastern flanks, that is, Tanzania craton and Mozambique belt respectively with evidence of faulting and lower crustal intrusions. The basement is overlain by Pliocene to Miocene volcanic and sedimentary rocks. Holocene sediments overlying widespread Pleistocene trachyte lavas generally cover the broader Magadi area (Githiri, Patel, Barongo, & Karanja, 2012). More structural studies inferred that evidenced North-South trending faulted escarpments and system control the occurrence of geothermal manifestations in the Magadi area and the zones extending towards the Nguruman escarpment (Riaroh & Okoth, 1994). Figure 2 is a geological lineaments map of the general Magadi area, while Figure 3 shows the spread of geological units over the entire study area. The maps indicate major faults oriented in the North-South direction with Lake Magadi to the east of the study area, locations of hot springs, and, an extensive lacustrine fluvial sediments zone to the west (Githiri, Patel, Barongo, & Karanja, 2011). The units found in the Kajiado zone could be linked to marble and quartzite units of Taita Hills through nappe folds (Bauernhofer et al., 2000). The fault orientations are significant in analyzing the rifting history as well as recharge routes for a geothermal system. The high rate of recent geothermal activity and volcanism related to geodynamic processes are well displayed in the Magadi region (Atmaoui & Hollnack, 2003), an indication of shallower structures yet to be investigated in detail (Kuria, 2011).

3. Methodology

3.1. Gravity Mapping

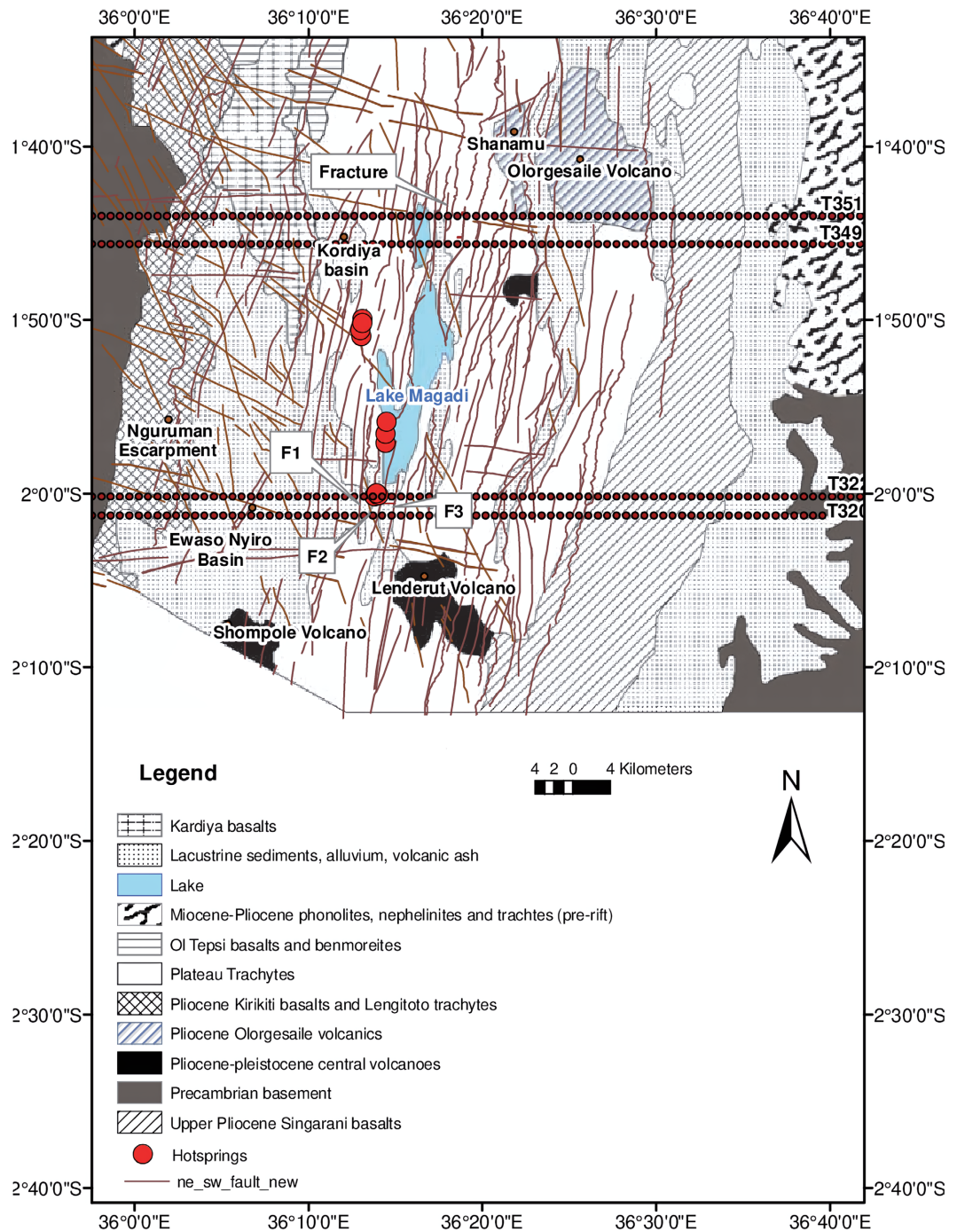The study area was subdivided into ten 8-km long transects along which

Figure 2. Key Features of Kenyan Southern Rift Zone, (b) ASTER DEM generated map (30 m resolution) of lineaments in Magadi and Nguruman Zone (Kuria, 2011).

measurement stations were determined with equal separation for uniform distribution as in **Figure 4**. Gravity measurement was done using a gravimeter of standard accuracy of about a microGal. The station coordinates were determined using a differential GPS. A total of 171 measurement stations plus several base readings were captured giving a data density of 2.375 stations/km². An absolute station at N: 9,794,120 and E: 187,060 with an observed gravity value of 977,718.2
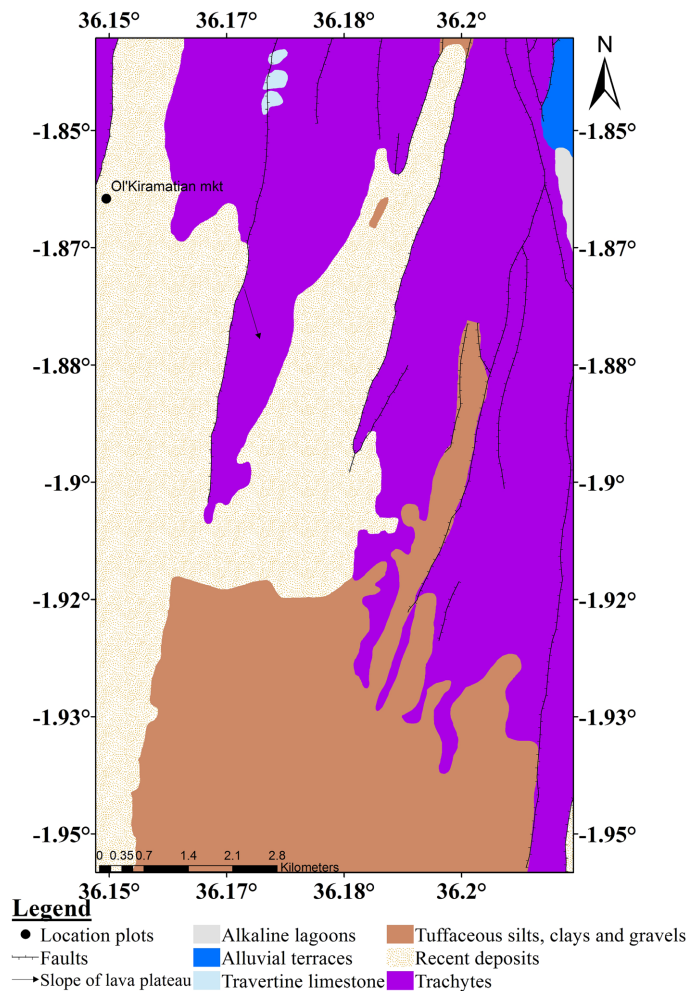
GEOLOGICAL MAP OF THE STUDY AREA

Figure 3. Main Geological units in the Magadi and Nguruman Zone.

was used as a base station. Observable geologic features at stations of measurements were noted for guided inference. To determine a complete Bouguer anomaly, the data were subjected to drift correction using base readings. The latitude effect was removed using Equation (1). Free Air correction (FAC) was made using the elevation-dependent Equation (2). Equation (3) was incorporated in the removal of the Bouguer slab before subjecting simple Bouguer anomaly to terrain correction using Equation (4), and an average rock density of 2.67 g/cm³ (Nyakundi, Githiri, & K'Orowe, 2020). By ordinary Kriging, a complete Bouguer anomaly (CBA) map was plotted for qualitative and quantitative analysis.

$$g_\phi = 9780318.5\left(1 + 0.005278895\sin^2\phi + 0.000023462\sin^4\phi\right)gu \qquad (1)$$

where ϕ is the latitude value in decimal degrees, and *gu* is gravity units.

$$FAC = \left(3.086 \times h\right)gu \qquad (2)$$
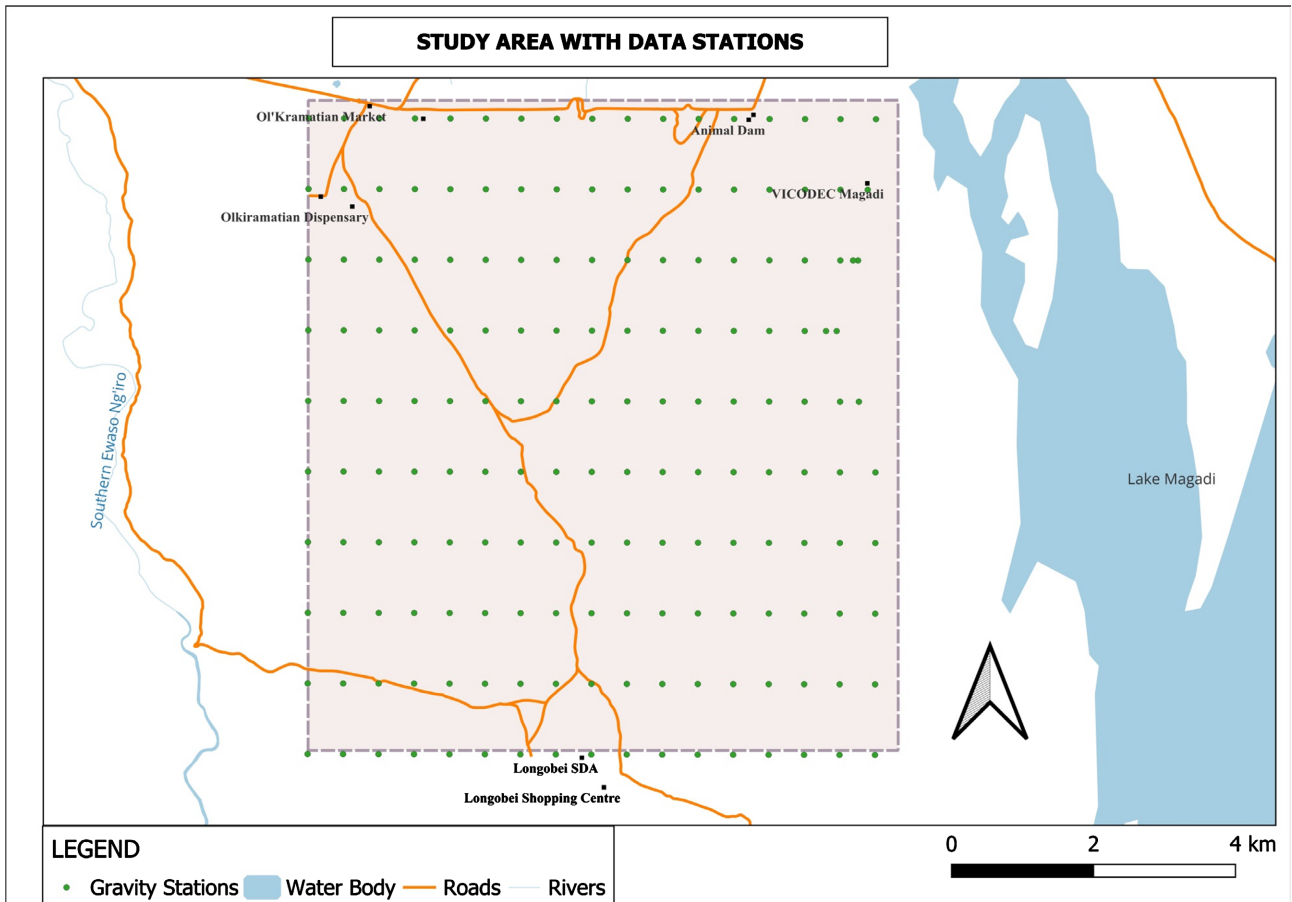
where *h* is the elevation in meters

Figure 4. Gravity Data Stations overlay on the Magadi-Nguruman Study Area.

$$BC = (0.4191\rho h)\, gu \qquad (3)$$

where ρ is the average rock density in g/cm³, and h is the elevation in meters.

$$T = 0.4191\frac{\rho}{n}\left(r_2 - r_1 + \sqrt{r_1^2 + z^2} - \sqrt{r_2^2 + z^2}\right) \qquad (4)$$

where T is the terrain correction for Hammer chat compartment, ρ is the average crustal rock density, n is the number of compartments in a Hammer chat zone, r_1 is the inner radius of the zone, r_2 is the outer radius of the zone, and z is the modulus of elevation difference between the data point and mean elevation of the compartment (Keary, Brooks, & Hill, 2002).

3.2. 3D-Euler Deconvolution

The standard 3D Euler method estimates the depth and position of anomaly source bodies.

Equation (5), known as Euler's homogeneity equation relates the potential field and its gradient components to the anomaly source location (Reid & Thurston, 2014). With the proper selection of structural index (N), Euler's equation was executed using a least squares method within a window thereby generating four unknowns (x, y, z, B) for the selected degree of homogeneity.

$$\left(x-x_0\right)\frac{\partial T}{\partial x}+\left(y-y_0\right)\frac{\partial T}{\partial y}+\left(z-z_0\right)\frac{\partial T}{\partial z}=N\left(B-T\right) \qquad (5)$$

where x_0, y_0, z_0 are the coordinates of the gravity anomaly source whose gravity vertical component T and regional value B are measured at (x, y, z) on the surface. N is the measure of the degree of homogeneity or structural index (Nyakundi, Githiri, & Ambusso, 2017; Keary, Brooks, & Hill, 2002).

The structural index as applied in Euler deconvolution is a measure of the rate of change of a potential field with distance. For the gravity field, the value ranges from 0 to 2 as illustrated in Table 1 (Githiri, Patel, Barongo, & Karanja, 2011). A Sill, Dike, or Step can be detected in the gravity field by using a structural index of 0.

In this study, a structural index of 0 was used in the determination of the Euler solutions over the complete Bouguer anomaly grid for 15% depth tolerance (Cooper, 2014), and an Euler plot was obtained. This was because the heat sources could be intrusive dike structures from magma chambers.

3.3. Spectral Analysis

Statistical power spectrum analysis has been applied to gravity data to determine the depths of gravity anomaly sources. Forward Fourier analysis was initially worked out to set gravity data into the frequency domain for easy transformation. For observed gravity anomaly, the power spectrum P_k is determined by Equation (6) (Nguimbous-Kouoh, Ngos III, Mbarga, & Manguelle-Dicoum, 2017).

$$P_k=\left(A_k\right)^2=\left(P_k\right)_0 \mathrm{e}^{\pm 2kz_t} \qquad (6)$$

where A_k is the amplitude coefficient of the spectrum, $k=2\pi/\lambda$ is the wavenumber (rad/km), and z_t is the estimated depth to the anomalous source body.

To obtain the plot of the power spectrum against the wavenumber linearly, the natural logarithm was applied on both sides of Equation 6 to get Equation (7).

$$\ln P_k = \ln\left(P_k\right)_0 \pm 2z_t k \qquad (7)$$

Half the gradient of the best line fit of the plot gives the average depth to the top of the anomalous source body (Abdullahi, 2022). Most spectral analysis cases have three segments displayed in the plot. The segments correspond to different

Table 1. Structural Indices for geological structures in a gravity field.

Structural Index	Body in Gravity Field
0	Sill/Dike/Step
0.5	Ribbon
1	Vertical pipe
2	Sphere

anomaly sources (Moral, Ortis, & Tejero, 2000). The segments are characterized by wavenumber intervals which directly relate to the average depth to the top of the source. The steepest segment corresponding to low wavenumber values reflects deeper or regional sources (Chen, Mou, & Meng, 2016). The high-frequency segment, normally at the tail end of the slope, is related to noise from data processing and is normally disregarded during interpretation.

4. Results and Discussion

4.1. Complete Bouguer Anomaly Maps

The complete Bouguer anomaly map with data stations is shown in Figure 5. The map displays a contour interval of 1 mGal with minimum contour at -198 mGals and maximum contour at −174 mGals. The eastern and southeastern zones of the study area display high gravity values ranging from −180 mGals to −174 mGals. This region neighbors locations of visible hot springs and Lake Magadi at about 2 km as shown in Figure 6. The gravity high values can then be
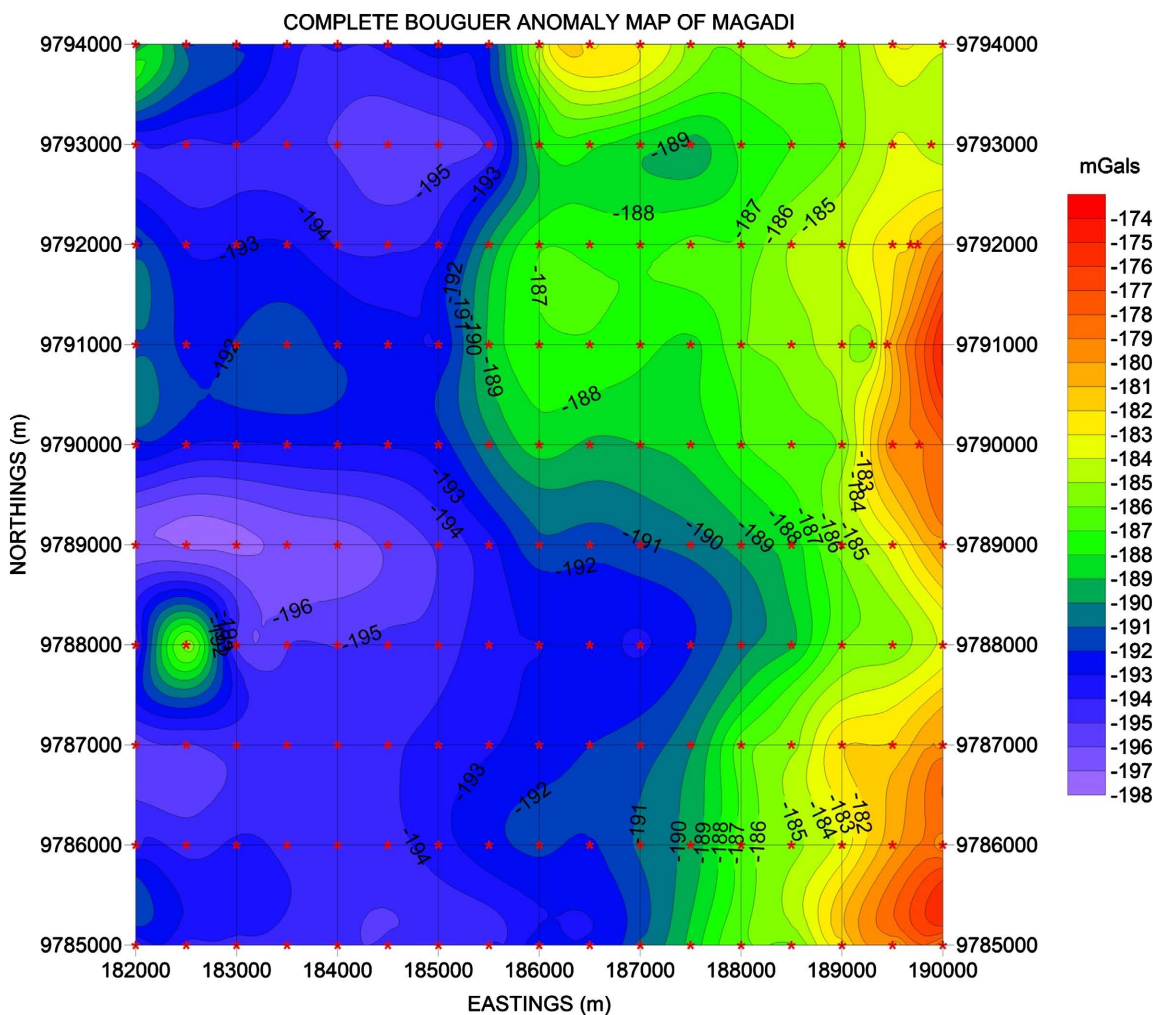

Figure 5. Complete Bouguer Anomaly map of Nguruman-Magadi area. The red dots are data stations. The contour interval is 1 mGal.
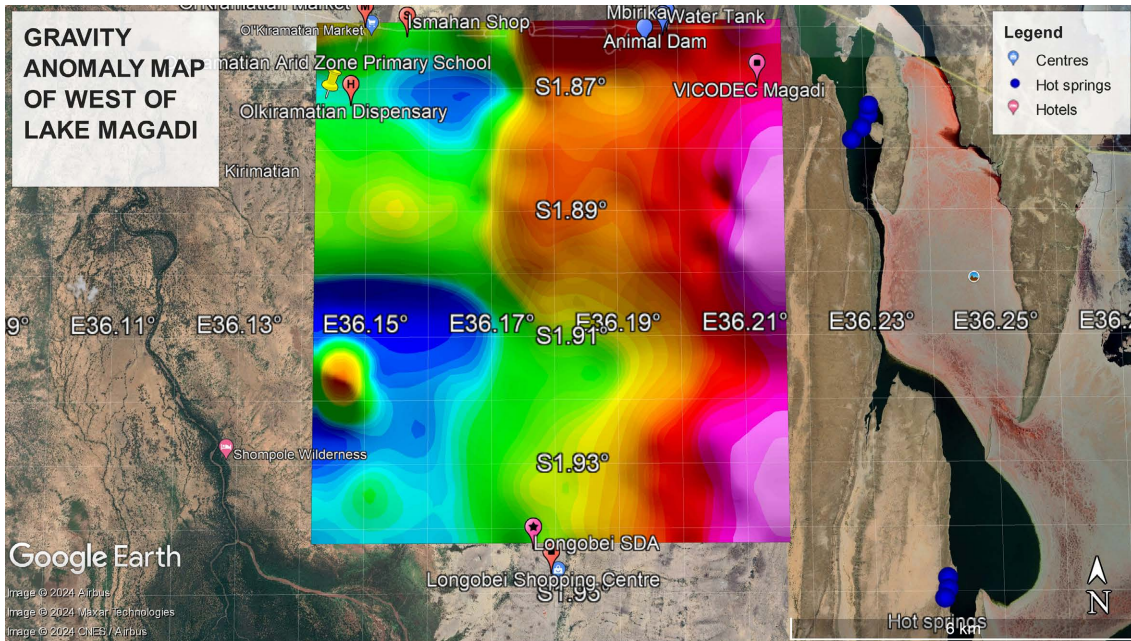
Figure 6. Gravity Anomaly Map overlay on Google Earth. Proximity to hot springs and Lake Magadi is ≈2 km.
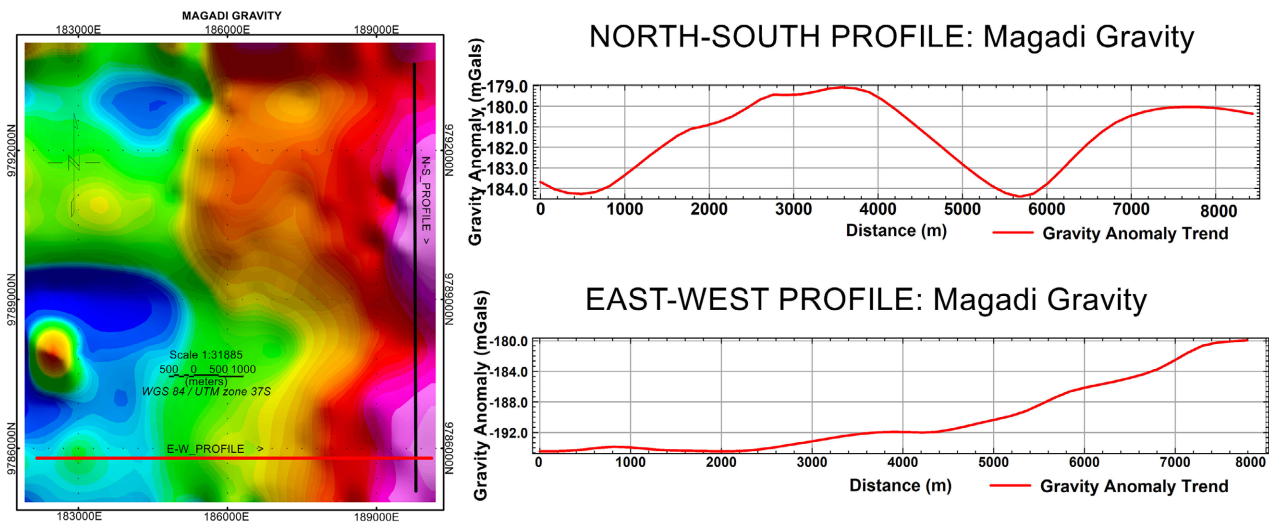

Figure 7. The cross-section profiles on the CBA map: (a) the distribution of gravity anomalies over the study area, (b) the North-south trend with two peaks of gravity high values. (c) The East-west profile with anomaly values ascending towards the east.

associated with cooling volcanic intrusives responsible for the evident surface manifestations of deep heating. The Olkiramatian area in the west of the study area is generally silent having relatively low gravity measurements ranging from −198 mGals to −191 mGals. **Figures 7(a)-(c)** show the location and trend of gravity anomaly as displayed by the cross-sections along E-W and N-S profiles for more qualitative interpretations. The association of gravity-high measurements with deep sources is more evident in the regions bounding Lake Magadi. The high gravity anomalies along the western flanks of Lake Magadi signify possible intrusions with densities higher than the average density of the crustal rocks (2.67 g/cm³). Previous studies involving forward modeling of gravity data with an aim of

mapping geothermal heat sources in an area within the rift confirmed the crucial relationship between the measured high gravity anomalies and shallow intrusive heat sources (Nyakundi et al., 2021). The intrusions characterize the heat flux patterns of a geothermal field. From the maps (Figure 5 and Figure 6), it is evident that the hot bodies spread more to the regions below the hot springs and the Lake. Few closed circular anomalies scattered over the study area show the long wavelength gravity anomalies in the Magadi area. CBA maps are useful in creating qualitative impressions of the desired source bodies. However, the maps cannot be used to obtain a comprehensive quantitative report. There is a need to integrate analytical methods for quantitative analysis. Other approaches may include full tensor gravity anomaly processing for subsurface structural features (Kebede & Mammo, 2021), and edge detection techniques for outlining gravity anomaly source boundaries (Oruc, 2010; Pham et al., 2020; Siombone et al., 2021; Siombone et al., 2022).

4.2. Euler Solutions

Figure 8 is a standard 3D Euler map of solutions to the depth of gravity anomaly sources for structural index $SI = 0$. The color variation represents changes in depth in meters. The deepest solutions were calculated at 744 m in the eastern
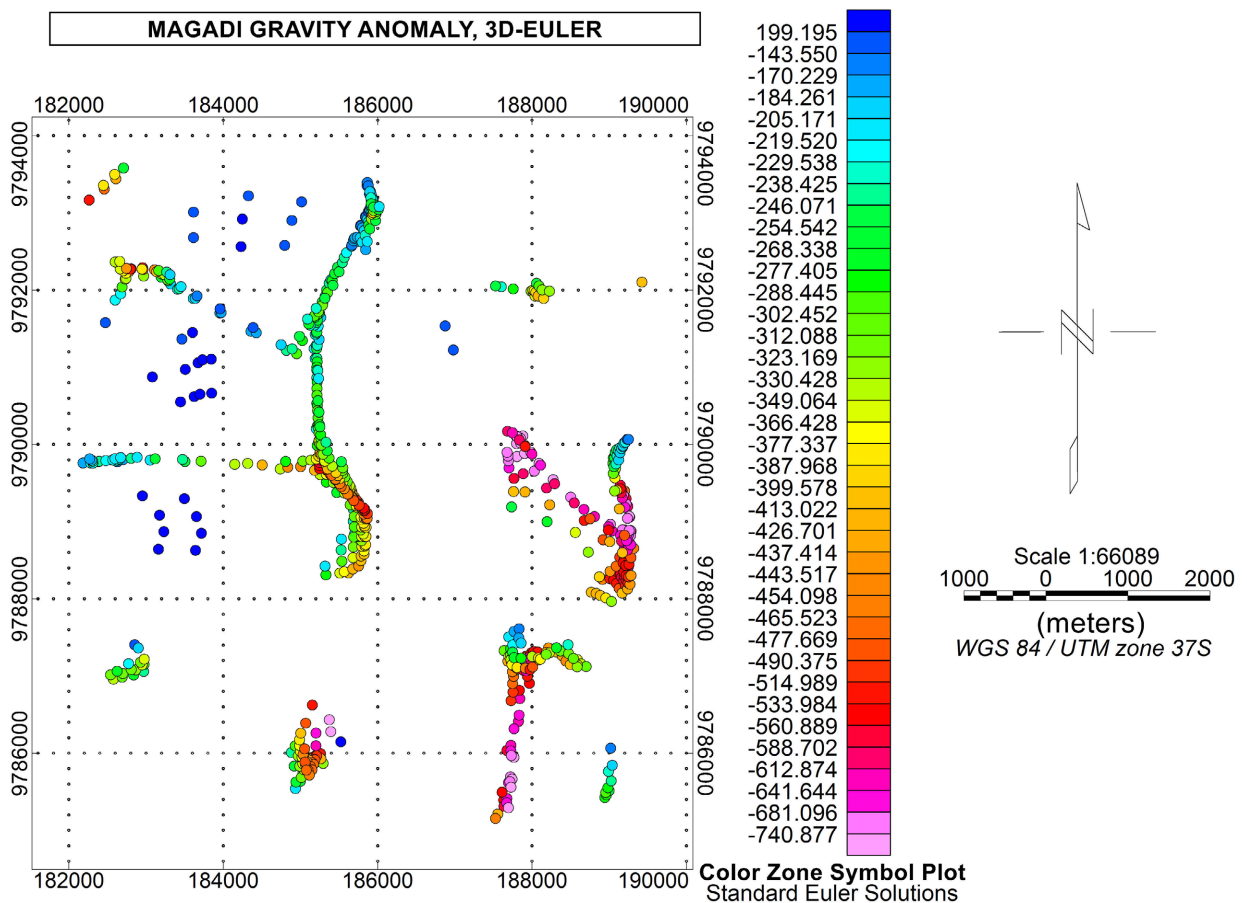

Figure 8. Standard 3D Euler solutions map for structural index $SI = 0$.

and southeastern areas of the map.

This synchronized with the CBA map (Figure 5) that placed the highest gravity anomalies in the same zone. Linear solutions at an approximate depth of 350 m were determined for a buried fault running North-South in the upper mid-section of the study area. The Euler solutions concentrate on zones of abrupt changes of gravity anomaly contours associated with contacts, steps, and faults. The southeastern solutions depict the edge of a possible high-density volcanic sill at about 0.8 km dipping towards the south of Lake Magadi. The inferred fault location and anomaly edges were verified by a horizontal derivative plot in Figure 9. The anomalies have a general North-South alignment, an observation that synchronizes with the trends of major and minor faults in the Magadi region (Riedl et al., 2022). Faults act as conduits for recharge in a geothermal system.
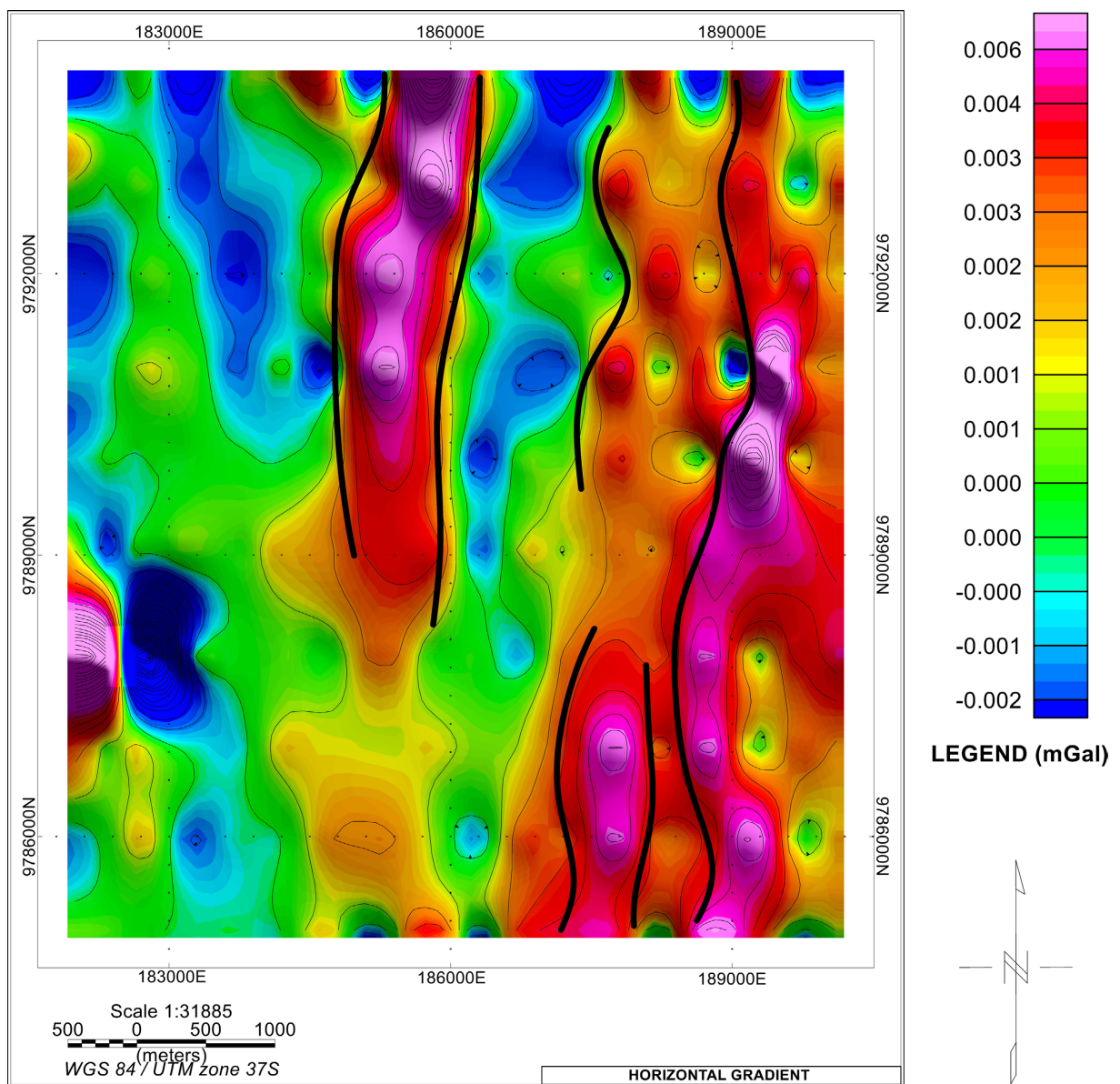

Figure 9. Horizontal gradient plot with inferred fault locations and Anomaly source edges.

4.3. Spectrum Analysis

Further analysis of depth to sources involved spectral analysis as shown in **Figure 10**. Taking the Magadi study area as one spectral block, values of wavenumber (k) and natural logarithm of the power spectrum $\left(\ln P_k\right)$ were calculated and plotted. Using Equation 7 the average depth to the top $\left(Z_t\right)$ of deep sources was found to be 5.8275 km while that to the top of shallow sources was found to be 2.4694 km. The deep sources were detected within the radial range of less than 0.5 rad/km (wavelength equal to or greater than 12.57 km). The radial range determining the depth of residual sources was found to be from 0.51 rad/km to 1.95 rad/km (wavelength between 12.32 km and 3.22 km) as shown in **Table 2**. The deepest sources can be associated with the Tanzanian Craton in the upper crust (Muirhead et al., 2016), as described in section 2.0.

The residual sources can be linked to high-density volcanic intrusion within the Magadi subsurface. The third segment with gentle gradient defined by
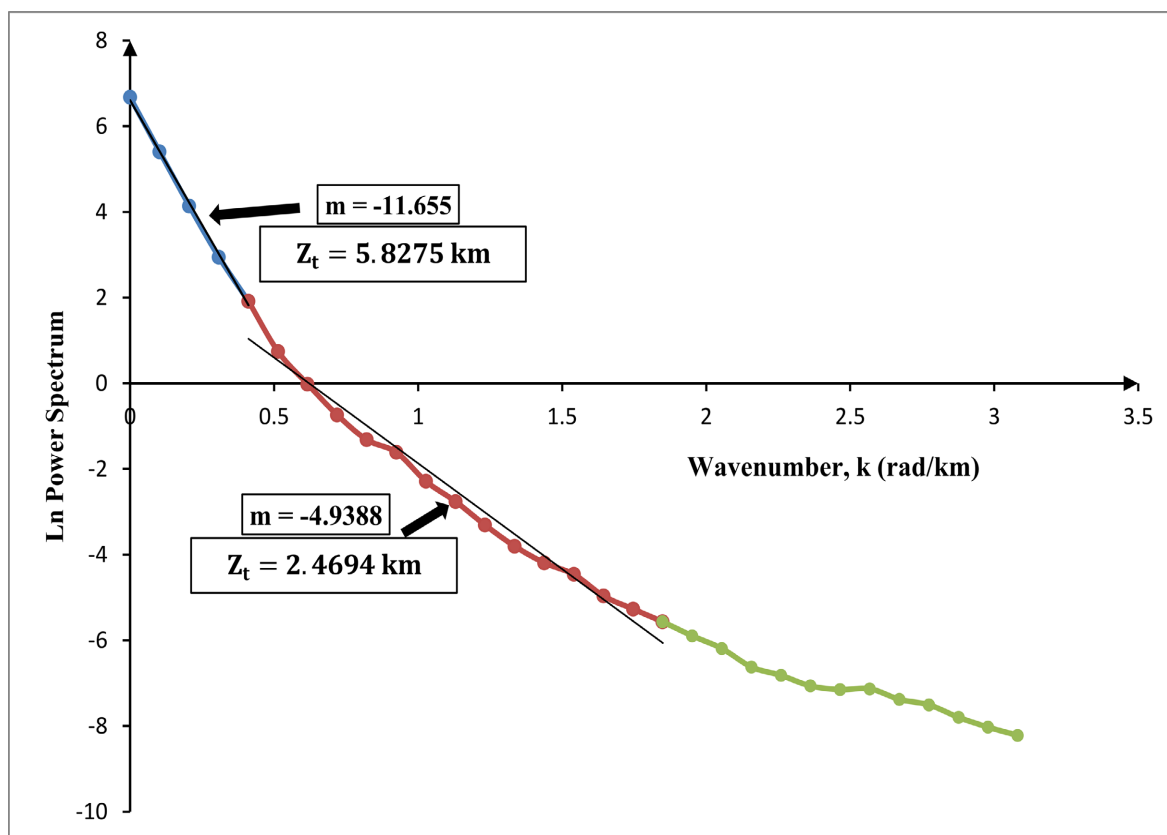

Figure 10. Power spectrum plot versus wavenumber for gravity map in **Figure 5**. Two different segments, regional, and residual are distinguished, and their mean depths are determined from the gradients of lines of best fit.

Table 2. Calculated depth to the top of gravity anomaly sources

Gravity Anomaly	Gradient, m ($2Z_t$)	Depth to top, Z_t (km)	Wavenumber, k (rad·km^{-1})	Wavelength, λ (km)
Shallow	−4.9388	2.4694	0.51 to 1.95	12.32 to 3.22
Deep	−11.655	5.8275	≤0.5	≥12.57

wavenumber values greater than 2 rad/km is regarded as noise from spectral analysis rounding errors, and geophysical data processing errors, among others (Setiadi, Widodo, & Nainggolan, 2021; Moral, Ortis, & Tejero, 2000).

5. Conclusion

This study aimed to investigate gravity anomalies in the Magadi region and understand their implications on geothermal systems. The processed gravity data successfully generated a detailed complete Bouguer anomaly map of the Magadi-Nguruman area. The map revealed high-density volcanic intrusions responsible for high anomalies in the eastern and southeastern zones of the study area with a −180 mGals to −174 mGals gravity anomaly range. The sedimentary basins of the Olkiramatia area to the west registered relatively low anomalies of −198 mGals to −191 mGals. 3D Euler solutions to depths of anomalies were calculated using a structural index of zero, delineating buried N-S trending fault at 350 m depth in the mid-upper region of the study area. The southeastern Euler solutions depicted the edge of a possible high-density volcanic sill at 0.8 km depth that dipped towards the south of Lake Magadi. Additionally, spectral analysis was done on the anomaly map for further depth screening, and deep and shallow anomaly sources were found at 5.8275 km and 2.4694 km respectively. The deep sources were linked to the Tanzanian craton basement within the upper crust whereas the residual sources were associated with high-density volcanic intrusions within the Magadi subsurface, a result that synchronizes with the geological findings in the area. The information on the location of the identified faults and volcanic intrusions is useful in the exploration of possible geothermal systems within the geological complexities of the Magadi area.

Acknowledgements

Special thanks to the National Oil Corporation of Kenya for software support. Greatly indebted to the Ministry of Geology and Mines for availing the geological report for the study area. I also recognize the support from the Department of Physics at the Jomo Kenyatta University of Agriculture and Technology.

Conflicts of Interest

The authors declare no conflicts of interest regarding the publication of this paper.

References

Abdullahi, M. (2022). *Gravity Anomaly and Basement Estimation Using Spectral Analysis.* IntechOpen. https://doi.org/10.5772/intechopen.99536

Alexander, K. B., Ussher, G., & Merz, S. K. (2011). Geothermal Resource Assessment for Mt Longonot, Central Rift Valley, Kenya. In *Proceedings of the GRC Annual Meeting* (pp. 23-26). https://www.researchgate.net/publication/229138350

Atef, H., El-Gawad, A. A., Zaher, M. A., & Farag, K. S. (2016). The Contribution of Grav-

ity Method in Geothermal Exploration of Southern Part of the Gulf of Suez-Sinai Region, Egypt. *NRIAG Journal of Astronomy and Geophysics, 5,* 173-185. https://doi.org/10.1016/j.nrjag.2016.02.005

Atmaoui, N., & Hollnack, D. (2003). Neotectonics and the Extension Direction of the Southern Kenya Rift, Lake Magadi Area. *Tectonophysics, 364,* 71-83. https://doi.org/10.1016/S0040-1951(03)00051-9

Bauernhofer, A., Hauzenberger, C., Wallbrecher, E., Hoinkes, G., Fritz, H., Loizenbauer, J. & Opiyo-Akech, N. (2000). Strain and Kinematic Analysis of Major Tectonostratigraphic Units from the Mozambique Belt of the Voi District, Southeast Kenya and the Pare-Usambara Mountains, Northeast Tanzania. *Journal of African Earth Science, 30,* 10.

Chen, Z., Mou, L., & Meng, X. (2016). The Horizontal Boundary and Top Depth Estimates of Buried Sources using Gravity Data and their Applications. *Journal of Applied Geophysics, 124,* 62-72. https://doi.org/10.1016/j.jappgeo.2015.11.003

Cooper, G. R. J. (2014). Euler Deconvolution in a Radial Coordinate System. *Geophysical Prospecting, 62,* 1169-1179. https://doi.org/10.1111/1365-2478.12123

Githiri, J. G., Patel, J. P., Barongo, J. O., & Karanja, P. K. (2011). Application of Euler Deconvolution Technique in Determining Depths to Magnetic Structures in Magadi Area, Southern Kenya Rift. *Journal of Agriculture Science and Technology, 13,* 142-156.

Githiri, J. G., Patel, J. P., Barongo, J. O., & Karanja, P. K. (2012). Spectral Analysis of Ground Magnetic Data in Magadi area, Southern Kenya Rift. *Tanzania Journal of Science, 38,* 1-14.

Keary, P., Brooks, M. & Hill, I. (2002). *An Introduction to Geophysical Exploration.* Blackwell Scientific Publications.

Kebede, B., & Mammo, T. (2021). Processing and Interpretation of Full Tensor Gravity Anomalies of Southern Main Ethiopian Rift. *Heliyon, 7,* e06872. https://doi.org/10.1016/j.heliyon.2021.e06872

Kuria, Z. N. (2011). *Seismotectonics of Active Faults: Magadi Fault System, Southern Kenya Rift.* Ph. D. Thesis, University of Twente.

Mariita, N. O., & Keller, G. R. (2007). An Integrated Geophysical Study of the Northern Kenya Rift. *Journal of African Earth Sciences, 48,* 80-94. https://doi.org/10.1016/j.jafrearsci.2006.05.008

Moral, C., Ortiz, D., & Tejero, R. (2000). Spectral Analysis and Gravity Modeling of the Almazan Basin (Central Spain). *Revista de la Sociedad Geológica de España, 13,* 131-142.

Muirhead, J. D., Kattenhorn, S. A., Lee, H., Mana, S., Turrin, B. D., Fischer, T. P., Stamps, D. S. et al. (2016). Evolution of Upper Crustal Faulting Assisted by Magmatic Volatile Release during Early-Stage Continental Rift Development in the East African Rift. *Geosphere, 12,* 1670-1700. https://doi.org/10.1130/GES01375.1

Nguimbous-Kouoh, J. J., Ngos III, S., Mbarga, T. N., & Manguelle-Dicoum, E. (2017). Use of the Polynomial Separation and the Gravity Spectral Analysis to Estimate the Depth of the Northern Logone Birni Sedimentary Basin (CAMEROON). *International Journal of Geosciences, 8,* 1442-1456. https://doi.org/10.4236/ijg.2017.812085

Nyakundi, E. R., Githiri, J. G., & Ambusso, W. J. (2017). Geophysical Investigation of Geothermal Potential of the Gilgil Area, Nakuru County, Kenya Using Gravity. *Journal of Geology and Geophysics, 6,* 2

Nyakundi, E. R., Githiri, J., & K'Orowe, M. (2020). Depth Estimation of Geothermal Heat Structures by Euler Deconvolution of Gravity Data at Eburru Area, Kenya. *Journal of Geoscience and Environment Protection, 8,* 148-158.

https://doi.org/10.4236/gep.2020.83011

Nyakundi, E. R., Gitonga, G. J., & K'Orowe, M. (2021). Simultaneous Modelling of Gravity and Magnetic Data in a Measured Heat Flux Area to Characterize Geothermal Heat Sources: A Case for Eburru Geothermal Complex, Kenya. *Journal of Geoscience and Environment Protection, 9,* 40-54. https://doi.org/10.4236/gep.2021.95005

Omenda, P. (2014). *Geothermal Country Update Report for Kenya.* Naivasha.

Omenda, P. A. (2007). The Geothermal Activity of the East African Rift. *Short Course II on Surface Exploration for Geothermal Resources, Organized by UNU-GTP and Ken-Gen,* Naivasha, 2-17 November 2007, 2-17. https://www.grocentre.is/gtp/moya/page/sc-05

Oruc, B. (2010). Edge Detection and Depth Estimation Using a Tilt Angle Map from Gravity Gradient Data of the Kozaklı-Central Anatolia Region, Turkey. *Pure and Applied Geophysics, 168,* 1769-1780. https://doi.org/10.1007/s00024-010-0211-0

Pham, L. T., Öksüm, E., Duc, T., & Vu, M. N. (2020). Comparison of Different Approaches of Computing the Tilt Angle of the Total Horizontal Gradient and Tilt Angle of the Analytic Signal Amplitude for Detecting Source Edges. *Bulletin of the Mineral Research and Exploration, 165,* 53-62. https://doi.org/10.19111/bulletinofmre.746858

Reid, A. B., & Thurston, J. B. (2014). The Structural Index in Gravity and Magnetic Interpretation: Errors, Uses, and Abuses. *Geophysics, 79,* J61-J66. https://doi.org/10.1190/geo2013-0235.1

Riaroh, D., & Okoth, W. (1994). The Geothermal Fields of the Kenya Rift. *Tectonophysics, 236,* 117-130. https://doi.org/10.1016/0040-1951(94)90172-4

Riedl, S., Melnick, D., Njue, L., Sudo, M., & Strecker, M. R. (2022). Mid-Pleistocene to Recent Crustal Extension in the Inner Graben of the Northern Kenya Rift. *Geochemistry, Geophysics, Geosystems, 23,* e2021GC010123. https://doi.org/10.1029/2021GC010123

Setiadi, I., Widodo, J., & Nainggolan, T. B. (2021). Geological Interpretation of Offshore Central Sumatra Basin using Topex Satellite Gravity data. *IOP Conference Series: Earth and Environmental Science, 944,* Article ID: 012034. https://doi.org/10.1088/1755-1315/944/1/012034

Simiyu, S. M., & Keller, G. R. (1998). Upper Crustal Structure in the Vicinity of Lake Magadi in the Kenya Rift Valley Region. *Journal of African Earth Sciences, 27,* 359-371. https://doi.org/10.1016/S0899-5362(98)00068-2

Siombone, S. H., Maryanto, S., & Wiyono, (2021). Bouguer Anomaly of Geothermal Reservoir at Tiris Area, Probolinggo, East Java, Indonesia. *Journal of Geography, Environment and Earth Science International, 25,* 1-18. https://doi.org/10.9734/jgeesi/2021/v25i930304

Siombone, S. H., Susilo, A., & Maryanto, S. (2022). Integration of Topex Satellite Gravity and Digital Elevation Model Shuttle Radar Topography Mission (DEM SRTM) Imagery for Subsurface Structure Identification at Tiris Geothermal Area. *Positron, 12,* 98-111. https://doi.org/10.26418/positron.v12i2.56880